# Some Aspects of Modelling Rock Fabric and Impact on Fluid Flow in Sandstone Reservoirs – Faults and Compaction

by Øystein Pettersen,
Centre for Integrated Petroleum Research,
Bergen, Norway

## Abstract

This paper addresses aspects of fluid flow related to rock fabric, that are difficult or impossible to model in a flow simulator by standard methods, but which may have significant impact on fluid flow. For some reservoirs, the described procedures will be a necessary ingredient in a simulation model if production history is to be validated and understood.
For flow across faults the standard model of defining sand-to-sand contacts with fault transmissibilities can be replaced by a more general procedure, based on recent studies of fault composition. The typical rock compaction model, where pore volume modifications are based on pore pressure, is generally not sufficiently sophisticated to predict actual pore volume and permeability changes during production. A systematic overview of different compaction causes and implications is given, accompanied by appropriate modelling aspects. Some results from reservoir rock parameter experiments are presented to support the theory, as well as examples from field simulations.

## Introduction

The influence of fault zone architecture on fluid flow in faulted reservoirs, and consequences of reservoir compaction during production are two elements of the reservoir rock state description that are of major significance for the recovery of oil and gas. Still, these features are frequently too simplistically represented in flow simulation models. This can partly be due to missing or poor data, but is often because the simulator itself is simplified or lacks capability to capture the effects associated with these features,

Furthermore for certain types of reservoirs, such as those with a high content of weak sands, experience has shown that over-simplification leads to highly erroneous flow simulation results.

Typically, available reservoir data is only a small subset of that required for a complete reservoir description. For mature reservoirs it is therefore standard procedure to validate the input data for models by *history matching*. History matching is the process by which the input data are tuned to match the known production history. During this procedure, a fundamental assumption is that the physics governing the fluid flow is accurately reproduced in the simulator, such that the simulator is capable of computing "correct" fluid flow if the input data are correct. However if this is not so, the value of the laborious data validating process will be severely reduced.

This paper addresses some issues of the modelling where either (1) the governing physical laws are not included in the simulator, or (2) they may be available but are cumbersome to use, and are therefore largely neglected. The aim of this paper is to describe these features and how they may be accounted for during the simulation process.

Studies through the last decade have revealed that flow through faults is far more complex than previously assumed. Manzocchi et. al. [Manzocchi 1999] demonstrate that the estimation of a priori transmissibility multipliers could be improved by taking into account the internal structure of the fault. The study is, however, restricted to fluid flow across sand-to-sand contacts. Hesthammer and Fossen [Hesthammer 2000] give an overview of different factors that influence fluid flow through faults, and associated uncertainties. That paper (and the references therein) and field experience clearly show that the sand-to-sand-contact flow assumption often is invalid. A more general approach to simulating flow across faults will be presented.

Compaction is often modelled with a constant compressibility, or as a tabulated function of fluid pressure in a flow simulator. Although such a model may be adequate for some studies, it has been established that compaction is also dependent on changes in the reservoir stress field, which cannot be computed by most reservoir simulators. Hence it has to be done by a stress simulator coupled to the flow simulator, see e.g. [Settari 1999], [Thomas 2003], [Gutierrez 1998].

In most reservoir simulation studies, permeability is treated as time-independent. It is now, however, generally accepted that permeability is dependent on compaction, the stress path, and stress dynamics during production. (e.g. [Koutsabeloulis 1998], [Yale 1998], [Gutierrez 1998].)

Examples on how these factors have been included in simulation studies will be shown, using

reservoir examples from offshore Norway, mostly from the Brent Group. The mechanical strength of the reservoirs varies from weak (loose sand) to strong (highly consolidated sandstone). The presented methods have been developed during data validation of several generations of simulation models from different fields. These studies have shown that fluid flow clearly was governed by some physical features that were not straightforward to model, especially in the reservoirs that are predominantly comprised of poorly consolidated sand.

## Fault flow modelling

When modelling fluid flow through faults where sand to sand contact is present, it is commonly assumed that fluids flow across the fault plane. Transmissibility multipliers are used to control the fault's resistance to flow, but the flow pattern is predetermined (Fig. 1).

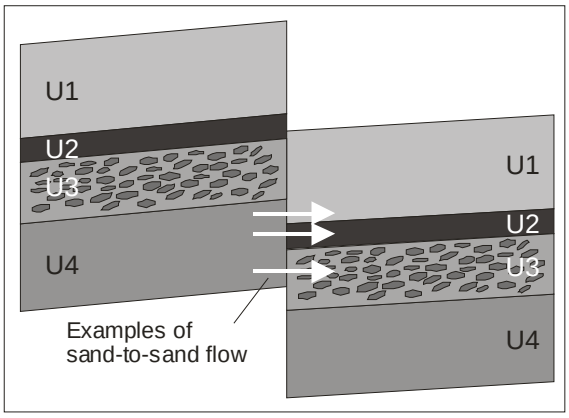


**Figure 1. The Standard Fault Model**

Many of the existing methods for assigning fault transmissibilites are based on the calculated shale content along the fault surface, either by using SGR (shale gouge ratio) or CSF (clay smear factor). This approach may apply to some faults, but is likely to provide inaccurate results when applied to faults with a heterogeneous internal structure [Knipe 1997].

In several of our previous simulation studies it was apparent from the observed water production history that fluids clearly traversed the fault zone by a more complex flow path. Hence, focus was shifted towards the understanding of flow through faults and feasible methods of simulating it.

Recent studies have shown that faults are far more complex than the simple model, e.g. [Caine 1996], [Hesthammer 2000]. Two structural components usually characterize fully developed fault zones: a fault core and a damage zone. Fault cores and damage zones show different permeability characteristics which are related to the different deformational features encountered within them. The fault core often consists of low-permeability rocks where slip is localized, whereas the damage zone consists of rock volumes affected by fault-related fracturing (e.g. shear bands) and folding (e.g. drag folds) (Fig. 2). The width of the damage zone appears to be roughly proportional to the throw of the fault [Knott 1994], [Hesthammer 2000].

When modelling fault flow in a simulator, it would be advantageous if the flow pattern and fault permeability could be determined by macroscopic parameters such as the fault throw, the clay content of the host rock and the net to gross ratio of the reservoir interval. As the damage zone contains shear bands and minor vertical and horizontal faults, the resulting flow will generally be along a tortuous path which cannot be predetermined in detail. Local sealing properties can be dependent on lithology, shear stress state, fluid saturations and temperature [Hesthammer 2002]. In ongoing research, the goal is to establish improved models for macroscopic flow patterns from detailed fault zone descriptions. Although flow on the microscopic level cannot be accurately modelled, it is assumed that most fault zones will include a typical distribution of low level attributes, hence allowing for upscaling.

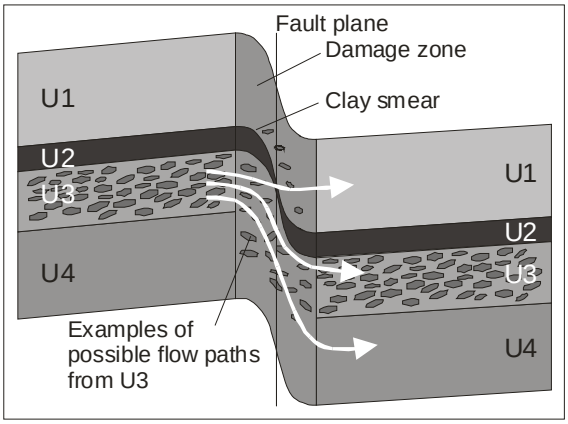


**Figure 2. General Fault Flow, Indicating Clay Smear and Gouge Ratio.**

Presently, the a priori assumptions for flow pattern and fault resistance will only be a starting point, while we have to rely on historical data to establish a reliable model, through history matching. This process is unfortunately not well suited for automated methods, and a great deal of manual effort is required, certainly dependent on the quality of the initial estimates.

In the Eclipse reservoir simulator, sand-to-sand contact fault transmissibilities are controlled by the keywords *MULTX* and *MULTY*, which is a convenient manner to control flow between cells which are geometric, but not necessarily grid-cell index neighbours. To define flow between cells which are geometrically separated, the general keyword *NNC* (Non-Neighbour Connection) can be used. This keyword sets up a flow connection between two arbitrary cells, as in

```
NNC I1 J1 K1 I2 J2 K2 TRAN,
```
whereby a connection is defined between the two cells with indices *(I1, J1, K1)* and *(I2, J2, K2)*, with an inter-cell transmissibility *TRAN* [Schlumberger 2003]. There are no restrictions on the cell indices, so any kind of connection can be set up. An obvious disadvantage is that presence of non-neighbour connections increases the size and complexity of the system of equations the simulator must solve. Hence, excessive use of NNC keywords can slow down the run considerably, but that cannot be avoided if correct fault flow is to be modelled.

In real reservoir studies, several thousand non-neighbour connections can be present. Definition of the NNC keywords and keeping the list of NNC data up-to-date during input data updates are hence tasks that are too large to be performed manually. The only practical means of organizing the input data is by user-developed software that allows for easy input, and writes the necessary Eclipse keywords.

**Procedure for generalizing permitted fault flow paths in Eclipse**

In this section a method for defining flow paths across a fault is described. The aim was to offer a user friendly means of setting up the flow parameters, such that the user can handle ordinary sand-to-sand connections and more complex flow patterns in the same fashion. Some examples of permitted fault flow paths are shown in Fig. 3, with a fault between cells with i-indices 14 and 15 (the separation between the cells are for illustrative purposes only). In the example, unit U3 is comprised of grid layers 4, 5, and 6, unit U4 of grid layers 7 and 8, and unit U5 of grid layer 9. Lines are drawn to identify all possible flow paths connecting U3 on the hanging wall side to U3 and U4 on the footwall side, and U4 (HW) to U5 (FW).

To simplify later computations it has been found advantageous to compute and store transmissibility estimates for *all possible* flow paths across the fault, as a one-time task. I.e. the *pseudo-transmissibilities* between *all cell pairs* in two neighbour cell columns separated by the fault are calculated, as if the cells were physical neighbours. For the configuration in Fig. 3, pseudo-transmissibilities would be computed for cell pairs (*i=14, j, k1*) and (*i=15, j, k2*), for all possible combinations of k1 and k2. These pseudo-transmissibilities can be computed in a straightforward manner, or improved estimates can be used, e.g. by the procedure proposed by Manzocchi et. al. [Manzocchi 1999], generalized to non-sand-to-sand-contact cells. (The quality of the pseudo-transmissibility estimates is not critical, since these will be modified by the user later.)

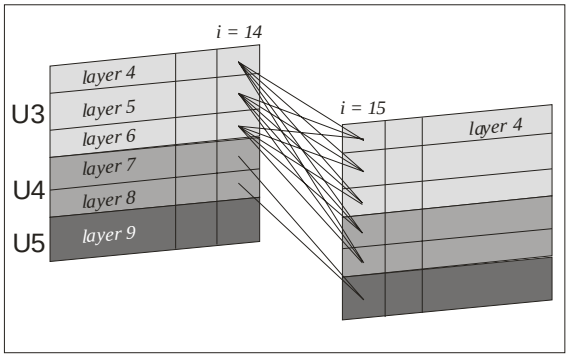


**Figure 3. Flow paths from U3 to U3 and U4, and from U4 to U5**

The flow path candidates are defined as cell column pairs separated by fault traces (similar to the Eclipse *FAULTS* keyword), where each fault cell will have an entry of the form *(i, j, direction)*, i.e. flow from cell *(i, j)* may flow through a fault in the defined *direction*. For the fault in Fig. 3, named *F4N*, assume that the shown cross-section is valid for *j = 12,13,...,25*. Then this part of the fault would be defined as

```
F4N 14 12 25 +x
```

Fluid may enter the fault from a layer *k1* on the hanging wall side, and exit to a layer *k2* on the footwall side. At this stage, all possible combinations *(k1, k2)* are considered as valid flow path candidates. The next task is to define the permitted flow paths that will actually be used in the simulation. This can be done on a layer by layer basis, using the (grid) layer indices, or by lumping layers into user-named flow regions.

The faults and flow region definitions are not static, and will commonly be redefined several times during a data validation process.

On use the fault flow parameters are entered in a spreadsheet, with syntax as shown in Fig. 4.

| #New Fault | #Fault name | |
|---|---|---|
| FAULT | F4N | |
| #Flow “from” | #Flow “to” | #Multiplier |
| U3 | U3 | 0.1 |
| U3 | U4 | 0.01 |
| U4 | U5 | 0.02 |
| ... | | |
| FAULT | F4S | #Next fault |

**Figure 4. Example of flow parameter spreadsheet. (# is used for comments).**

This example corresponds to Fig. 3, where each cell connected to fault F4N and belonging to region U3 on one side of the fault will connect with all cells belonging to region U3 on the other side, defined by relevant NNC keywords. The inter-cell transmissibility (“fault transmissibility”) will be 0.1 times the computed pseudo-transmissibility. For

connections to region U4 on the "receiving" side the multiplier will be 0.01, etc.

The sand-to-sand contact connections can be handled automatically by Eclipse, but it is more user-friendly to let the software handle *all* connections. Then the user does not need to be concerned with the kind of connections that are involved in each case.

A technical consideration is that connections which are *logical* neighbours (i.e. cell *indices* are adjacent, but cells need not be in geometric contact, as cells (*i=14, k=5*) and (*i=15, k=5*) in Fig. 3), will not be defined by non-neighbour connections, but by the keyword MULTIPLY, as in

```
MULTIPLY TRANX I J K MULTIPLIER.
```

(or similar for *TRANY*). This is automatically taken care of by the software.

Cells with zero permeability will generate a vanishing pseudo-transmissibility, and thereby be blocked for flow irrespective of geometry and multipliers, and hence need no special treatment.

Using the example data from Fig. 3, the software would write keywords as below, for use by Eclipse. Fault F4N separates grid cell columns (*i=14, j=21*) and (*i=15, j=21*), i.e. F4N is on the '+x' side of cell (*i j*) = (*14,21*) for all layers *k*. Then all connections (*i=14, j=21 ,k=k1*) to (*i=15, j=21, k=k2*) for any combination of *k1 k2*, will be fault connection candidates. For the example, let some pseudo-transmissibilities be defined by

({(i, j); (direction); (k1, k2) ; pseudo-tran})

```
{(14, 21); '+x'; (4, 4); 10000}
{(14, 21); '+x'; (4, 5);  5000}
{(14, 21); '+x'; (4, 6);  7500}
```

Then an excerpt of the generated Eclipse keywords would be:

In the NNC-file:

```
NNC
   14 21 4  15 21 5  500  /
   14 21 4  15 21 6  750  /
```

In the MULTTRAN-file:

```
MULTIPLY
  TRANX  14 21 4  0.1  /
```

The described procedure applies for static fault transmissibilities. It has also been observed that fault transmissibilities may change during production. For example an initially sealing clay barrier can fail if the differential stress across the barrier exceeds the failure level, as defined by an appropriate failure criterion. While this phenomenon can be modelled in an ad hoc fashion by using history data, the physical reasoning will generally be poorly based. If fault transmissibilities are believed to be dynamic, the failure criteria should be computed by a coupled stress and flow simulator (see below).

## Compaction

Compaction in poro-elastic or poro-plastic media is defined as a change in the pore volume caused by change in confining pressure or pore pressure. Since compaction is one of the most important energy suppliers in a producing reservoir, quality estimates of compaction development have great economic significance in addition to the theoretical interest. Compaction can be difficult to estimate from production data, especially during unloading (pressure-buildup) as it depends, in a non-trivial manner, on stress state dynamics and stress path. A good qualitative description has been given by Fjær et. al. [Fjær 1992], and a computational procedure based on a coupled stress-flow simulator was described by Settari and Walthers [Settari 1999].

Examples of measurements of Young's modulus *E* for sandstones and sands are shown in Figs. 5 and 6. (Performed by Statoil and ERMC (Edinburgh Rock Mechanics Consortium, comprised of groups from Heriot-Watt University and University of Edinburgh)). The trends which can be seen in these figures seem to be typical for sandstones and sands, as similar results were observed in a large number of tests taken from different North Sea sandstone reservoirs.

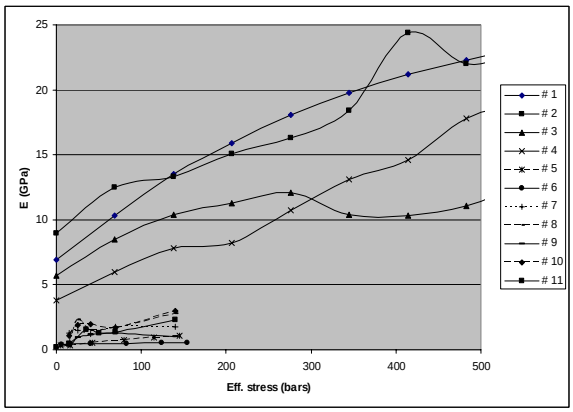


**Fig. 5. Young's Modulus *E* vs. effective axial stress $\sigma'_a$ for sand and sandstone samples of varying strength**

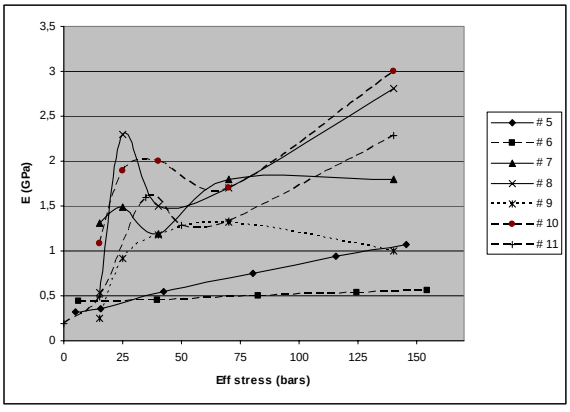


**Fig. 6. As Fig. 5, zoomed in on the weaker sands**

In general, Young's modulus $E$ is clearly dependent on applied uni-axial stress, and except for the weakest sands, $E$ increases with load, i.e. the rock grows stronger, or hardens. Moreover, on average, $E$ increases faster for larger initial values of $E$.

Weaker sands appear to have a less regular behaviour under load (Fig. 6). The intuitive explanation is that the samples fracture after a moderate load, and then harden under continued loading.

The initial values of $E$ are at least an order of magnitude smaller than Young's modulus for the sand grains, which signifies that the compression of the sample is only insignificantly governed by grain compression. Denote the grain compression coefficient by $K_s$, and the bulk compression by $K_b$. Then Biot's constant $\alpha$ is defined by

$$\alpha = 1 - \frac{K_s}{K_b} \qquad (1)$$

[Fjær 1992]. The *effective stress* $\sigma'$ is defined as

$\sigma' = \sigma - \alpha p_f$,

where $\sigma$ is the total stress, and $p_f$ the fluid pore pressure. $\alpha$ is normally taken as unity for sands, which by Eq. (1) is equivalent to assuming that grain compression can be neglected compared to pore space compression. (See also [Chuhan 2002].) Adopting this assumption, changes in effective stress will be equal to changes in fluid pressure when the total stress is constant.

The standard compaction model offered by most flow simulators is as a table of pore volume multipliers vs. pore pressure. It has, however, been experimentally verified, and generally accepted that soil / sand response is determined by the effective stress [Wood 1990]. The flow simulator compaction model is hence only approximate, unless total stress is constant, which will seldom or never be fulfilled. If actual, observed rock behaviour in reservoirs is to be modelled correctly, the reservoir simulator must be coupled to a stress simulator which calculates the stress field and resulting deformations, from which compaction can be inferred.

**Elements of compaction**

A control volume $V_b$ with a pore volume $V_p$ and solid volume $V_s$ has porosity $\phi = V_p / V_b$. By compaction we understand a change of $V_p$ due to a change of the stress in the control volume. The pore volume changes are composed of different elements, as described in the following, where the assumption that grain compression can be neglected is adopted.

**Grain packing reorganization**

Consider first a sandstone or sand which hardens during compaction, corresponding to an increasing Young's modulus. Since the grains themselves are not, or only insignificantly compressed when effective stress is increased, the observed reduction in pore volume can only be caused by a tighter packing of the grains. The reorganizing of grains will constitute an increasingly more stable packing. Since the grains will tend to remain at the most stable packing, previous packing patterns will not be regained on subsequent unloading. Hence, the compression will result in permanent deformation of the pore space. Moreover, the grain packing and resulting pore space will at all times be determined by the historical maximal stress level. Since each level of grain packing is tighter than previous levels, further packing will be increasingly harder to achieve. Hence material hardening is to be expected during loading, as observed in Figs. 5 and 6.

Following [Wood 1990], an elasto-plastic model for the sand can be constructed. Each incremental increase of mean effective stress

$$p' = \frac{1}{3}(\sigma'_{xx} + \sigma'_{yy} + \sigma'_{zz}) \qquad (2)$$

results in a "new" material with no memory of its past states. This material is characterized by its current grain packing (and value of $E$). As long as $p'$ does not exceed its historical maximal value $p'_M$, the material will behave elastically with constant volume loading-reloading. Once $p' > p'_M$ the material attains a new state by plastic deformation, following the normal compression line (Fig. 7). This line can be used as a pore volume multiplier function for flow simulation, if the approximation $\Delta p' \approx \Delta p_f$ is acceptable ($\Delta$ denotes change). The constant-volume unloading-reloading must be handled by defining the compaction curve as irreversible.

The minimum volume limit in Fig. 7 corresponds to a (theoretical) state where further grain packing is not possible. In this stage, which is unlikely to occur for values of $p'$ normally encountered during production, grain compression or crushing may occur, factors which are not accounted for in the described model.

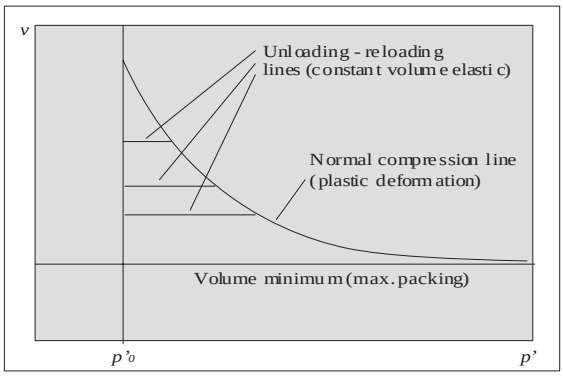


**Fig. 7. Compaction: Specific volume *v* vs. mean effective stress *p'***

Each material state is associated with a yield surface in the $p'$-$q$ plane, where $q$ is the deviatoric stress (a measure for the difference between maximum and minimum stress components) (Fig.

8). For (*p'*, *q*)-values within the yield surface, the material will behave elastically. When (*p'*, *q*) touches the yield surface, the material will yield, whereby it enters a new state ("new material") with redefined elasto-plastic parameters and its own associated yield surface, which necessarily must be outside the previous one. A significant feature of the material in question is that the initial yield surface must pass through the point ((*p'*$_0$, *0*), where *p'*$_0$ is the initial mean effective stress (or the historical maximum if the reservoir has experienced larger effective stresses than the present). Thereby yielding will occur once the mean effective stress exceeds its initial value.

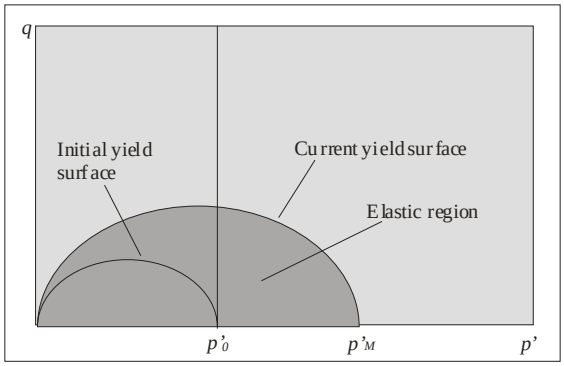


**Fig. 8. Compaction: Yield surfaces in p'-q space.**

When the grains reorganize to a tighter packing by sliding and rotating, the pore space itself is changed, a process which can be described as pore wall failure. This may seem like a contradiction; the material fails continuously at pore volume level while growing stronger (hardening) on bulk volume level. But failure cannot occur if not proceeded by material weakening. The dual level approach is the key to the understanding of the compaction process. The standard sample testing provides the necessary elasto-plastic parameters, while the theoretical grain model is the basis for concluding that plastic behaviour (with permanent deformation) must be expected.

The current grain packing pattern is determined by the effective stress $\sigma'_M$, and also by existence of bonding agents, which may be weakened by changes in fluid composition, especially water content.

Assume the grain packing geometry is defined by a function $\Gamma = \Gamma(\sigma', S_w)$, where $S_w$ is water saturation. The pore volume is then defined by the (unknown) function $\Gamma$, and a change in pore volume is the sum of the macro-level bulk volume change and low level effects,

$$\delta V_p = \delta V_B(\sigma) + \frac{\partial V_p}{\partial \Gamma}\delta\Gamma(\sigma', S_w) \qquad (3)$$

The second term in Eq. (3) cannot easily be computed, and current research is directed towards a better understanding of this mechanism. Presently, it is handled as an unknown perturbation to the pore volume reduction, which has to be estimated by a data validation process.

By the argument above, and also supported by field experience, this kind of compaction is totally irreversible, i.e. pore volumes will at all times be at their historical minimum, at least as long as the fluid pressure remains below the initial value.

When a control volume compacts, the relation $V_b = V_s + V_p$ must always be fulfilled. Since the grains were assumed incompressible, $V_s$ will not change, and hence the reductions in bulk volumes and pore volumes are equal. As each control volume can be compressed but not expand, the total reservoir volume must be reduced during compaction (disregarding swelling, which is not likely in sands or sandstone). A consequence of this is that the surrounding rock must expand or swell. From experience and geomechanic simulations most of the expansion will be located to the overburden. Hence, for sandstone reservoirs, subsidence must be expected at top reservoir level. (The overburden may expand or be rigidly displaced, so subsidence at sea floor level need not be significant.)

**Material weakening and rock fabric failure**

Assume now that the porous material is weakened during compression, whereby typically Young's modulus will be decreasing with effective axial stress $\sigma'_a$. Such a behaviour can be an indication that the material is continuously fracturing during increased loading. In tests where rock weakening was observed, *E* was typically an order of magnitude smaller than in the rock hardening cases (Fig. 6).

If the differential stress in the control volume exceeds the failure level as designated by a failure criterion, the macroscopic material will fracture. Depending on the type of failure the material will develop stable fractures, or dependent on the plastic flow conditions, sand grains can break loose from the pore walls. The sand will either settle in the pores, or be transported by the flowing fluid as an additional fluid phase, with saturation $S_s$. This is generally a very complex situation to describe. Generalization of the fluid mass balance equations to include a sand phase is straightforward, but the transport equation for the sand phase is not obvious. If the sand can be immediately removed, as e.g. in the vicinity of a wellbore, the criterion would simply be that the sand phase is spontaneously produced by a sink term, as described by Wan and Wang [Wan 2001]. In reservoir regions far away from wells, the transport term would probably need to include a modification of the failure criterion in neighbouring control volumes. This matter is still the focus of research. While the process of sand failure can be computed by the stress simulator, the sand transport at present cannot. We can, however, state that by failure the pore volume will be increased by a volume equal to that transported out of the control volume. Extending the geometry function $\Gamma$ to also

be dependent on the solid mass $m_s$ in the control volume the pore volume change due to failure will be directly related to porosity change,

$$\delta V_p = \frac{\partial \phi}{\partial \Gamma} \delta \Gamma [\Delta \sigma', \delta m_s(\Delta \sigma')] \quad (4)$$

where $\delta m_s$ is the mass of removed sand and $\Delta\sigma'$ is the differential stress $(\sigma'_{max,h} - \sigma'_{min,h})$. Note that although fracturing and sand transport may increase $\phi$ locally, the grain packing reorganization which occurs simultaneously will normally result in a total reduction of pore volume.

This effect is of course irreversible.

**Grain Compression**

Grain compression must be taken into account if Young's modulus for the bulk porous material is of the same order as for the grains. This is, however, an exceptional situation in sand or weak sandstone reservoirs.

The change in pore volume by grain compression alone is described by standard theory. Often linear compaction can be assumed, as in [Wang 2000],

$$\delta V_p = C_p V_p \delta \sigma' \quad (5)$$

or in general a nonlinear dependence,

$$\delta V_p = f_g(V_p, \sigma') \quad (6)$$

which can be elastic or elasto-plastic. The compressibility coefficient $C_p$ in equation (5) is typically determined by uni-axial compression tests.

**Total compaction – practical considerations**

The total compaction can in theory be found by combining the three factors defined by equations (3) – (6), given by a general expression of the kind,

$$\frac{\partial V_p}{\partial t} = f \left\{ \frac{\partial V_B}{\partial \sigma}\frac{\partial \sigma}{\partial t} + \frac{\partial V_p}{\partial \Gamma}\left( \frac{\partial \Gamma}{\partial \sigma'}\frac{\partial \sigma'}{\partial t} + \frac{\partial \Gamma}{\partial S_w}\frac{\partial S_w}{\partial t} \right) + \frac{\partial \phi}{\partial \Gamma}\left( \frac{\partial \Gamma}{\partial (\Delta \sigma')} + \frac{\partial \Gamma}{\partial m_s}\frac{\partial m_s}{\partial (\Delta \sigma')} \right)\frac{\partial (\Delta \sigma')}{\partial t} + \frac{\partial f_g}{\partial \sigma'}\frac{\partial \sigma'}{\partial t} \right\} \quad (7)$$

or

$$\frac{\partial V_p}{\partial t} = f^* \left( \frac{\partial \sigma}{\partial t}, \frac{\partial \sigma'}{\partial t}, \Delta \sigma', \frac{\partial (\Delta \sigma')}{\partial t}, \frac{\partial S_w}{\partial t} \right) \quad (8)$$

Since the function $f$ (or $f^*$) in general is unknown, the actual dependency of $\delta V_p$ on the parameters can only be determined by running coupled stress – flow simulations. However, even if an exact computation of the development of compaction in time and space were possible, it would require detailed knowledge of all necessary poro-elasto-plastic parameters, and like the petrophysical parameters these are in general only known at sparse points in the reservoir. Compaction derived from the historical production data will therefore typically deviate somewhat from the simulated one, due to the incomplete stress field description and the possible micro-level effects in Eq. (8). Data validation is therefore used to adjust the simulated compaction, defined by pore volume multipliers.

An example of simulated vertical displacement along a cross-section at top reservoir level is shown in Figure 9, with displacements at five different times (each "Tstep" is six months). Note that the cross section also includes sideburdens.

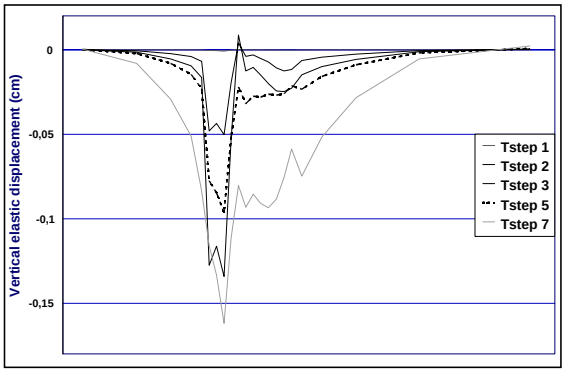


**Figure 9. Vertical displacement at top reservoir along an E-W cross section**

In fluid flow simulators, such as Eclipse, the pore volume multipliers (and associated permeability multipliers) are defined as functions of pore pressure alone. This will generally be an over-simplification, as discussed. Nevertheless, using such relationships is the general rule, and often satisfactory results are achieved. The pore volume multipliers are typically determined by historical data from a pure loading process, which does not give any information on whether the compaction is reversible. This is a critical question since it directly affects the amount of pressure support that can be expected from subsequent injection wells. By the arguments in previous sections it is often possible to arrive at a relatively reliable decision based on the elasto-plastic parameters. By the grain packing argument, compaction in sand or weak sandstone reservoirs should normally be classified as irreversible. This recommendation has been supported by a number of history matching studies in Brent Group reservoirs, when data from unloading (reservoir pressure build-up) became available.

## Coupled Rock Mechanics Simulation

By the preceding discussion, the only consistent way to calculate the pore volume multipliers is by coupled stress – fluid flow simulations.

The rock mechanics simulations were run on the finite element stress simulator VISAGE™ from VIPS [VIPS 2003]. (For other descriptions of

coupled simulations see also [Thomas 2002], [Koutsabeloulis 1998].)

Running a *fully* coupled simulation, i.e. where the flow and stress equations are solved simultaneously is obviously the most correct procedure. However, such simulations are very time-consuming. Furthermore, no simulator exists which includes both an advanced stress-solver, and the freedom to define production options which exist in most commercial flow simulators. Fully coupled runs were therefore not included in the reported studies.

A typical coupled run scheme was to run the Eclipse flow simulator for six months (production time), then let VISAGE™ compute the resultant stress field and derived grid cell pore volumes and permeabilities, which were then used to pseudo-initialize Eclipse for running the next six months.

The loosely coupled scheme is less CPU-time demanding than a fully coupled scheme, but has the disadvantage that material balance is not conserved between the flow simulation cycles, as the sudden changes in pore volumes alter the cell pressures. The lengths of the flow simulation periods were chosen such that these pressure changes remained small. A fully coupled run of this nature normally requires five to ten times the computing time of a pure flow simulation. Consequently it is desirable to keep the number of the times the full run is performed low. Our experience was that in a data validation procedure, it was advantageous to convert the results of the coupled runs to tables used directly by Eclipse. Only after significant changes in the input data was the full scheme repeated. When the data validation was found satisfactory, all further runs were done by Eclipse alone, with compaction tables as delivered by the final coupled runs.

## Subsidence-induced creep

A North Sea, Brent Group reservoir was produced on an averagely decreasing pressure for four years, where after a period of over-injection to rebuild pressure was commenced. Fig. 10 shows simulated and measured pressures for a typical flow region. The simulated pressure (dashed line in Fig. 10) is the best match that could be achieved after more than 200 data validation iterations.

When attempting to simulate the pressure changes through time, the main parameters that were varied were the (standard) compaction curves (i.e. compressibility vs. fluid pressure), aquifer size and aquifer to reservoir connectivity, and relative permeability curves. (All petrophysical and rock parameters were assumed constant in time.) Irreversible compaction curves were used (i.e. no pore volume recovery on unloading), and aquifer parameters were varied far outside "realistic" values. After attempting to match the pressure profile by all conceivable means, it was concluded that it could not be done by a traditional approach. As the general picture was the same for all flow regions the explanation could not be energy transfer between regions, but it appears there is insufficient energy in the reservoir during unloading (pressure build-up).

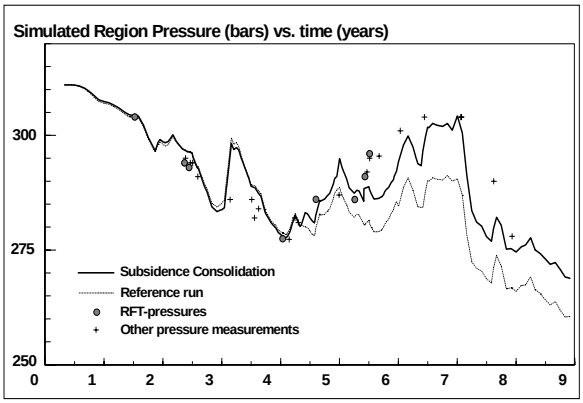


**Figure 10. Region Pressure profiles with and without subsidence-induced creep**

As mentioned above, it is not possible to determine compaction behaviour during pressure build-up (unloading) from production data gained during a pressure reduction period (loading). In this particular case we would expect pore space collapse to be the main factor, but the compaction curves could also partly include a contribution from aquifer inflow. Since subsidence could not be ruled out as a factor of influence, GPS measurements of sea floor depth were performed. Over a period of six months a vertical displacement of six cm. was observed.

Having established that a small degree of subsidence actually occurred, a consequence of this could be that the reservoir was exposed to subsidence-induced creep, as described by de Waal and Smits [de Waal 1985]. The pragmatic explanation was that once the overburden started moving, a stabilization or even increase in fluid pressure would not be sufficient to stop the movement, or reverse the subsidence.

To test the theory, the simulated displacement growth (Fig. 9) was extended in time with decreasing impact. I.e. from year 4 (Fig. 10), the reservoir was assumed to continue compacting, even though reservoir pressure was increasing. The influence of this creep induced compaction was assumed to reduce exponentially with time. The result of this modification to the simulation model can be seen in figure 10, the solid curve. Clearly the lack of energy has been accounted for. Although still not *proved*, the observed data and the failure to match pressure by other means is a strong indication that this is actual behaviour.

## Stress Dependent Permeability

It should be expected that the mechanism of grain reorganization affects permeability as well as pore volumes. Measurements of permeability vs. axial effective stress show a wide range of results, from

almost no effect to considerable permeability reduction.

Fig. 11 is an example of results from experiments performed by ERMC on weak sandstone cores from a Brent Group reservoir. In addition to the large reduction in permeability under load, it is seen that almost no permeability is regained during unloading, which supports the assumption that the compaction is plastic. (Note the similarity to Fig. 8)

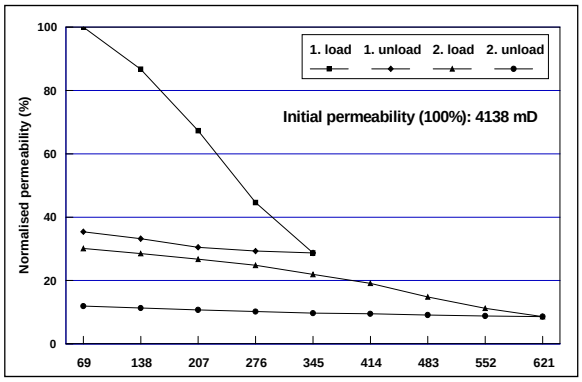


**Figure 11. Permeability variation vs. $\sigma'_a$ (bars) from core test**

The same kind of rock response has also been observed by field measurements. Fig. 12 shows permeability as measured by six (numbered) transient tests in the same well during a period of 21 months, vs. reservoir pressure. [Statoil 1992]

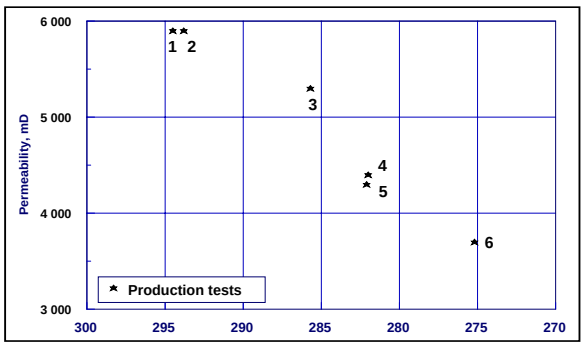


**Figure 12. Permeability vs. Pressure (bars) from six transient well tests during 21 months**

The results demonstrate that permeability can be, and often is stress dependent. The largest effects were seen in weak sands, which was to be expected.

For reservoirs which are comprised of sands with stress dependent permeability, the consequences of producing at low reservoir pressure should be investigated in advance. The obvious general loss of conductivity will not necessarily imply reduced production rates. A potentially more severe factor is the additional pressure drawdown near production wells, which can result in dramatically reduced well inflow potential. Such an effect has actually been observed in a small isolated fault block in a Brent Group reservoir.

The fault block was planned to be produced by an injector – producer pair WP and WI. To increase initial production rates both wells were put on production for six months, where after well WI was converted to an injector. At drilling time WI was tested for an injectivity index corresponding to an injection rate of at least 3500 SM3/day. However, when the well was put on injection, surprisingly the actual maximum injection rate after a while was only about 200 SM3/day.

To test if the low injection potential could be explained by permeability reduction the simulation model for the fault block was run with and without stress dependent permeability. Results from the simulations can be seen in Figures 13 and 14.

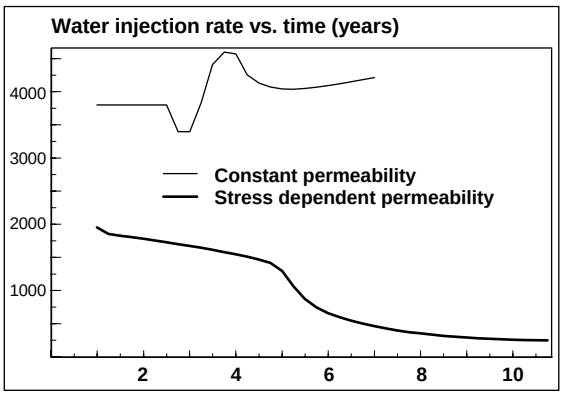


**Figure 13. Effect of stress dependent permeability. Simulated injection rates**

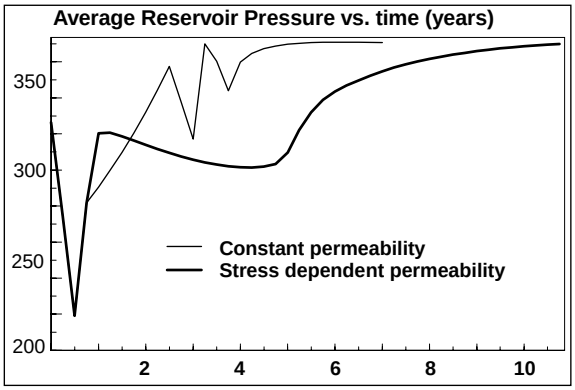


**Figure 14. Effect of stress dependent permeability. Simulated reservoir pressure**

As can be seen in the figures, without permeability reduction, the simulated injection rate stayed at its initial level. The simulated rate was, however, severely reduced when permeability was modelled as stress-dependent. This is clearly due to the reduced near-well permeability caused by the low reservoir pressure which was allowed to develop in the non-injection period.

## Conclusions

We have described how a traditional approach to modelling fault flow and compaction can be too simplistic to capture actual rock characterization and behaviour during fluid flow. Further we have also demonstrated practical means of adjusting the simulator input data to counter this, and that an extension of the simulation tool box and *modus operandus* is necessary when the flow is governed by fundamental physics which the flow simulator is incapable of handling.

Examples of experimental results demonstrate that the modifications are appropriate for relevant reservoirs.

## Acknowledgements

I would like to thank Statoil for providing some of the data used in the study, and the professors John Howell, Johnny Hesthammer, and Tore Skar, an for their helpful contributions and discussions.

## References

Caine 1996: Caine, J. S., Evans, J. P., Forster, C.B., Fault zone architecture and permeability structure, *Geology* **24**(11), 1025-1028

Chuhan 2002: Chuhan, F. A., Bjørlykke, K., Evidence of Grain Crushing during mechanical Compaction of Reservoir Sandstones – A Comparison with Experimental Results, *AAPG Ann. Meeting, Houston, Texas,* Mar. 10-13, 2002

de Waal 1985: de Waal, J. A., Smits, R. M. M., Prediction of reservoir compaction and surface subsidence: Field application of a new model, *SPE 14214, SPE ann. meeting, Las Vegas, Sept. 1985*

Fjær 1992: Fjær, E., Holt, R. M., Horsrud, P., Raaen, A. M., Risnes, R., Petroleum Related Rock Mechanics, *Developments in Petroleum Science, 33, Elsevier,* 1992

Hesthammer 2000: Hesthammer, J., Fossen, H., Uncertainties associated with fault sealing analysis. *Petroleum Geoscience*, **6**, 2000, 37-45
Hesthammer 2002: Hesthammer, J., Bjørkum, P. A., Watts, L., The Effect of temperature on sealing capacity of faults in sandstone reservoirs: Examples from the Gullfaks and Gullfaks Sør fields, North Sea, *AAPG Bulletin,* **v 86,** no **10** (Oct. 2002), 1733-1751.

Gutierrez 1998: Gutierrez, M., Lewis, R. W., The Role of Geomechanics in Reservoir Simulation, *SPE/IRSM 47392, Proc. Eurock 98, 2, Trondheim, Norway, July 8-10,* 439-448

Knipe 1997: Knipe, R. J., Juxtaposition and seal diagrams to help analyze fault seals in hydrocarbon reservoirs, *AAPG Bulletin,* **v. 81**, 187-195

Knott 1994: Knott, S. D., Fault zone thickness versus displacement in the Permo-Triassic sandstones of NW England, *J. Geological Soc. of London* **151**, 17-25

Koutsabeloulis 1998: Koutsabeloulis, N. C., Hope, S. A., "Coupled" Stress/Fluid/Thermal Multi-Phase Reservoir Simulation Studies Incorporating Rock Mechanics. *SPE/IRSM 47393, Proc. Eurock 98, 2, Trondheim, Norway, July 8-10,* 449-454

Manzocchi 1999: Manzocchi, T., Walsh, J. J., Nell, P., Yielding, G., Fault Transmissibility multipliers for flow simulation models. *Petroleum Geoscience,* **5,** 1999, 53-63

Schlumberger 2003: Eclipse Reference Manual.

Settari 1999: Settari, A, Walthers, D. A., Advances in Coupled Geomechanical and Reservoir Modeling With Applications to Reservoir Compaction. *SPE 51927, Proc. The 1999 SPE Reservoir Simulation Symposium, Houston, Texas, Feb. 14-17.*

Statoil 1992: Transient test analysis reports well XX (anonymised).

Thomas 2003: Thomas, L. K., Chin, L. Y., Pierson, R. G., Sylte, J. E., Integrating Geomechanics in Full-Field 3-D Reservoir Simulation – Modeling Techniques and Field Applications, *SPE Appl. Techn. Workshop, Corpus Christi, Texas, Jul. 31. – Aug. 1., 2003.*

VIPS 2003: The VISAGE™ System. User's Guide, V.I.P.S Ltd., 2003

Wan 2001: Wan, R. G. and Wang, J., Analysis of sand production in unconsolidated oil sand using a coupled erosional-stress-deformation model. *Proc. of the Canadian International Petroleum Conference 2001,* Calgary, Canada, June 10-12, 2001

Wang 2000: Wang, H. F., Theory of Linear Poroelasticity with Applications to Geomechanics and Hydrology, *Princeton University Press* 2000

Wood 1990: Wood, D.M., Soil Behaviour and Critical State Soil Mechanics, *Cambridge University Press*, 1990

Yale 1998: Yale, D.P., Crawford, B., Plasticity and Permeability in Carbonates: Dependence on Stress Path and Porosity. *SPE/IRSM 47582, Proc. Eurock 98, 2, Trondheim, Norway, July 8-10,* 485-494